OCA 999
pp: 1–14 (col.fig.: Nil)
PROD. TYPE: COM
ED: Selva
PAGN: Sabari – SCAN:

OPTIMAL CONTROL APPLICATIONS AND METHODS
Optim. Control Appl. Meth. (2011)
Published online in Wiley Online Library (wileyonlinelibrary.com). DOI: 10.1002/oca.999

Toward a generalized sub-optimal control method of underactuated systems

J. Patricio Ordaz-Oliver[1,*,†], Omar J. Santos-Sánchez[1] and Virgilio López-Morales[2]

[1]*Automatic Control Department, CINVESTAV, México Distrito Federal, México*
[2]*Centro de Investigación en ~~Tecnologí as~~ de Información y Sistemas, Universidad Autónoma del Estado de Hidalgo. Carr. Pachuca-Tulancingo Km. 4.5, 42184, Pachuca, Hgo. Mexico*

SUMMARY

In this paper, some experimental results and a performance analysis of a general control methodology for swinging up and stabilizing underactuated two-link robots are presented. The analyzed methodology is based on Euler–Lagrange dynamics, passivity analysis, and dynamic programming theory. The applied control method preserves the general structure of a suboptimal control approach, while the functional defining a performance index is based on the underactuated system energy. In order to illustrate the presented approach, the swing up and stabilization control of two experimental electromechanical underactuated systems about an unstable equilibrium point are shown. Copyright © 2011 John Wiley & Sons, Ltd.

Received 6 August 2009; Revised 19 January 2011; Accepted 19 January 2011

KEY WORDS: dynamic programming; sub-optimal control; experimental underactuated systems; passivity; Pendubot; rotatory pendulum

1. INTRODUCTION

Underactuated robots are well-known benchmark systems [1], where the problems of regulation on a set-point, swinging up and balancing around an equilibrium point, as well as trajectories tracking becomes a challenge. For years the swing up and stabilization control laws of underactuated robots have been divided into two structures: the first one to balance up to upper position and the second one to stabilize it at this position [2, 3]. The underactuated robots control systems studied in the literature by different approaches involve two switching controls [4–8], the first one swinging up the system to upper unstable equilibrium point and the second one to balance it about this equilibrium. This kind of approaches are discontinuous and involves global closed-loop stability problems; thus, the stability analysis becomes local.

The rigid-body mechanics of robot manipulator motion or flight control is often formulated with the general equation obtained from Lagrangian mechanics:

$$D(q)\ddot{q}+C(q,\dot{q})\dot{q}+G(q)=\tau. \tag{1}$$

The position coordinates $q\in\mathbb{R}^n$ with associated velocities $\dot{q}$ and accelerations $\ddot{q}$ are controlled via the vector $\tau\in\mathbb{R}^n$ of driving forces [6]. The generalized moment of inertia $D(q)\in\mathbb{R}^{n\times n}$ is a

*Correspondence to: J. Patricio Ordaz-Oliver, Universidad Politécnica de Pachuca, Facultad de Mecatrónica, Ex Hacienda Sta. Bárbara, Municipio de Zempoala, Hgo. 43830. Mexico.
†E-mail: jpordaz@ctrl.cinvestav.mx

symmetric and positive definite matrix, the Coriolis, centripetal forces $C(q,\dot{q})\dot{q}$, and the gravitational forces $G(q)$ all vary along the system trajectories. From the Euler–Lagrange formulation, (1) can be generally written as follows:

$$\frac{\mathrm{d}}{\mathrm{d}t}\begin{bmatrix} x_1 \\ x_2 \end{bmatrix} = \begin{bmatrix} x_2 \\ D(x_1)^{-1}[\tau - C(x)x_2 - G(x_1)] \end{bmatrix}, \tag{2}$$

where $x \in M \subseteq \mathbb{R}^{2n}$, $x_1 = q \in \mathbb{R}^n$, $x_2 = \dot{q} \in \mathbb{R}^n$, and $\tau \triangleq u \in \mathbb{R}^n$ is the control input. Since our problem formulation is given for stability around an equilibrium point, x_{eq}, then the nonlinear system (2) is rewritten as:

$$\dot{\tilde{x}} = f(\tilde{x}) + g(\tilde{x})u, \tag{3}$$

where $\tilde{x} = x - x_{\text{eq}}$. Based on dynamic programming and passivity concepts, in a recent contribution [9], a suboptimal control law is proposed. Where an approximation of Bellman function as a Lyapunov function is introduced. Taking the system passivity property and by using dynamic programming, the synthesis of a nonlinear control law is achieved. In order to figure out the nonlinear control law, it is necessary to solve first, a Linear Quadratic Regulator (LQR) from the linearized system of (3) and then, a Ricatti equation. These results are then used to find a useful Lyapunov function for the global nonlinear system. This methodology becomes quite involved for systems with higher degrees of freedom (DOF). Thus, it is quite illustrative, to reveal some computing details, to figure out this general methodology, via some physical implementations. This contribution aims to explicitly solve the control law problem, and give some guidelines to physical implementations on electromechanical benchmarks. This paper is organized as follows: In Section 2, the suboptimal control method is presented in a general framework. In Section 3, the method is constrained to 2 DOF under actuated robots and completely solved. In Section 4, some experimental results and comparison against numerical simulation, for 2 DOF well-known robots, are presented. Finally, Section 5 give some concluding remarks.

2. SUB-OPTIMAL CONTROL LAW (FULLY ACTUATED CASE)

Recently, a swing up and stabilization control law has been presented with a non-switching control law (swinging and stabilizing up [9]). Up to our knowledge, this technic is a novel approach, involving a complete analysis of a global single control law to swinging and stabilize an underactuated system. The Lyapunov function given on [9] is defined by:

$$V(\bar{x}) = \frac{1}{2}k_E\tilde{\mathscr{E}}(\bar{x})^2 + \frac{1}{2}\bar{x}^{\mathrm{T}}\underbrace{\begin{bmatrix} \bar{P}_{11} & \bar{P}_{12} \\ \bar{P}_{21} & \bar{P}_{22} \end{bmatrix}}_{\bar{P}}\bar{x} \in \mathbb{R} \tag{4}$$

where $\bar{x} = [\bar{x}_1, \bar{x}_2]^{\mathrm{T}} \in \mathbb{R}^{2n}$, $\bar{x}_1 = x_1 - x_{1\text{eq}} \in \mathbb{R}^n$ is the angular position error, $\bar{x}_2 = x_2 - x_{2\text{eq}} \in \mathbb{R}^n$ is the angular velocity error, $P \in \mathbb{R}^{2n\times 2n}$ is a strictly positive definite matrix, $\bar{P}_{12} = \bar{P}_{21}^{\mathrm{T}}$, $\tilde{\mathscr{E}} = \mathscr{E} - \mathscr{E}_{\text{eq}}$, $\mathscr{E}(\bar{x}) = K(\bar{x}) + U(\bar{x}_1)^{\ddagger} \in \mathbb{R}$ is the system total energy about the desired controllable equilibrium point, $K(\bar{x})$ is the system kinetic energy, $U(\bar{x}_1)$ is the potential energy about the desired controllable equilibrium point, and k_E is a positive energy gain.

Note that our approach is based on dynamic programming and Euler–Lagrange system properties with the advantage of global asymptotic stability [9], where the control law has the following structure:

$$u = -R^{-1}\{k_E\tilde{\mathscr{E}}(\bar{x})\bar{x}_2 + D^{-1}(\bar{x}_1)[\bar{P}_{12}^{\mathrm{T}}\bar{x}_1 + \bar{P}_{22}^{\mathrm{T}}\bar{x}_2]\}, \tag{5}$$

‡ $K(\bar{x}) = \frac{1}{2}\sum_{i=1}^{n} m_i v_i^2 = \frac{1}{2}x_2^{\mathrm{T}}D(x_1)x_2$; $U(\bar{x}_1) = \sum_{i=1}^{n} m_i h_i g$ where $h_i \in R^n$ are the ith height of the ith link respect to the mass center, and g is the gravitational constant. Finally, $\mathscr{E}_{\text{eq}} = \mathscr{E}(x)|_{x=x_{\text{eq}}}$.

DOI: 10.1002/oca

where $\bar{P}_{12}$, $\bar{P}_{22} \in \mathbb{R}^{n\times n}$ are symmetric and positive definite matrices, $R \in \mathbb{R}^{n\times n}$ is a positive definite diagonal matrix. Then, the control law to be applied for each link can be obtained as follows:

$$u = -k_E \tilde{\mathscr{E}}(\bar{x}) R^{-1} \bar{x}_2 - k(\bar{x}) \begin{bmatrix} \bar{x}_1 \\ \bar{x}_2 \end{bmatrix}, \quad k(\bar{x}) \in \mathbb{R}^{n\times 2n} \tag{6}$$

where $k(\bar{x}) = [k_1(\bar{x}), k_2(\bar{x})]$, reads:

$$k(\bar{x}) = [R^{-1} D^{-1}(\bar{x}_1) \bar{P}_{12}^{\mathrm{T}} \quad R^{-1} D^{-1}(\bar{x}_1) \bar{P}_{22}^{\mathrm{T}}]. \tag{7}$$

In order to solve the former nonlinear control law (in $\bar{P}_{12}$ and $\bar{P}_{22}$), it is necessary to solve a variant Ricatti equation. Instead of this, we can obtain an approximated solution around the equilibrium point, which must coincide with the steady-state solution of the Ricatti equation. The key idea of our method follows.

Observe that the nonlinear control law (6) applied to the system (3) about an unstable equilibrium point of the system seems similar to an LQR controller in a neighborhood of the equilibrium point; i.e. when $x \to x_{\mathrm{eq}}$. Assume that the linearization of the nonlinear system (3) is observable and controllable. Then, a result can be formally stated in the following:

Proposition 2.1 (*Patricio Ordaz-Oliver et al.* [*9*] *Nonlinear system approximation*)
Consider that the system (3) is linearized around an equilibrium point (stable or unstable). Assume that the linearized system is controllable. Then the control law (6) follows a reference and around the equilibrium point, it holds:

$$\lim_{x\to x_{\mathrm{eq}}} \left(-R^{-1} k_E \tilde{\mathscr{E}}(\bar{x}) \bar{x}_2 - k(\bar{x}) \begin{bmatrix} \bar{x}_1 \\ \bar{x}_2 \end{bmatrix} \right) \approx 0 - \lim_{x\to x_{\mathrm{eq}}} (k(\bar{x})) \approx -R^{-1} B^{\mathrm{T}} \bar{P} \bar{x}, \tag{8}$$

where $B \in \mathbb{R}^{2n\times n}$ is the linear representation of $g(x)$, and $\bar{P} \in \mathbb{R}^{2n\times 2n}$ is a matrix gain given by the steady-state Riccati solution. Additionally the following approximation is fulfilled:

$$\lim k(\bar{x})|_{x\to x_{\mathrm{eq}}} \approx R^{-1} B^{\mathrm{T}} \bar{P}. \tag{9}$$

The gains can be obtained from (9) (via an LQR solution), and then we replace this solution in the nonlinear control law (6)–(7).[§]

Remark 2.1
Proposition 2.1 is used in order to obtain the whole set of parameters of the nonlinear control (5), due to the matrix $\bar{P}$ can be straightforward obtained by solving the steady-state Riccati equation, and the elements R and B are given.

Remark 2.2
The parameter k_E is chosen heuristically. Observe that the term $R^{-1} k_E \tilde{\mathscr{E}}(\bar{x}) \bar{x}_2$ is zero when $x \to x_{\mathrm{eq}}$.

In this paper by simplicity and exposition clarity, the two-link swing up and stabilization control problem is explicitly solved, because when the DOF becomes higher, the gain choice is hindered.

3. UNDERACTUATED 2-LINK ROBOT DYNAMICS

The standard general dynamic equations are given by (1), but when they have the underactuated property, i.e. n is bigger than the number of control inputs, then the system can be rewritten as follows:

$$D(\hat{q})\ddot{\hat{q}} + C(\hat{q}, \dot{\hat{q}})\dot{\hat{q}} + G(\hat{q}) = \tau, \tag{10}$$

[§]This solution gives the $\bar{P}_{12}$ and $\bar{P}_{22}$ matrix values.

DOI: 10.1002/oca

where $\hat{q} = [q_a, q_u]^{\mathrm{T}}$, q_a is the actuated variable, and q_u is the underactuated variable. For a two DOF, when the first joint has the actuator and the second link is the underactuated joint, the classical underactuated model has the following structure:

$$\underbrace{\begin{bmatrix} d_{11} & d_{12} \\ d_{21} & d_{22} \end{bmatrix}}_{D(\hat{q})=D(x_1)} \underbrace{\begin{bmatrix} \ddot{q}_a \\ \ddot{q}_u \end{bmatrix}}_{\ddot{\hat{q}}=\dot{x}_2} + \underbrace{\begin{bmatrix} c_{11} & c_{12} \\ c_{21} & c_{22} \end{bmatrix}}_{C(\hat{q},\dot{\hat{q}})=C(x)} \underbrace{\begin{bmatrix} \dot{q}_a \\ \dot{q}_u \end{bmatrix}}_{\dot{\hat{q}}=x_2} + \underbrace{\begin{bmatrix} g_1 \\ g_2 \end{bmatrix}}_{G(\hat{q})=G(x_1)} = \underbrace{\begin{bmatrix} u \\ 0 \end{bmatrix}}_{\tau} \tag{11}$$

Or from (2) it can be rewritten as follows [6]:

$$\frac{\mathrm{d}}{\mathrm{d}t} \begin{bmatrix} x_{1a} \\ x_{1u} \\ x_{2a} \\ x_{2u} \end{bmatrix} = \begin{bmatrix} x_{2a} \\ x_{2u} \\ D(x_1)^{-1} \left[\begin{bmatrix} u \\ 0 \end{bmatrix} - C(x) \begin{bmatrix} x_{2a} \\ x_{2u} \end{bmatrix} - G(x_1) \right] \end{bmatrix}. \tag{12}$$

The control law (6) in closed loop with (12) holds the following proposition for two link vertical underactuated robots.

Proposition 3.1 (*Underactuated 2-link control solution, Patricio Ordaz-Oliver et al.* [9])
If the system is underactuated as in (11), the control law for the actuator is given by:

$$u = -\frac{k_E \tilde{\mathscr{E}}(\bar{x})}{\det(R)} r_{22} \bar{x}_{2a} - \sum_{j=1}^{4} k_{1j}(\bar{x}) \bar{x}_j, \tag{13}$$

where $\bar{x}_{2a}$ is a scalar, and

$$k_{1j}(\bar{x}) = \frac{d_{22} \bar{p}_{j3} - d_{21} \bar{p}_{j4}}{r_1 \det(D(\bar{x}))}, \tag{14}$$

where $\bar{p}_{j3}, \bar{p}_{j4}$ are the entries of matrix $\bar{P}$ used in (4).[¶]

For a detailed proof of this proposition please refer to [9]. In order to illustrate our control approach, let us give a numerical and experimental example which is applied on two well-known 2-DOF robot platforms (Pendubot and Rotatory pendulum system).

4. EXPERIMENTAL RESULTS

In this section, the experimental setup and system realization are described for two underactuated systems, and then the experimental data are discussed and analyzed.

4.1. Hardware

Two-DOF underactuated robots are used as benchmark to test our methodology (Figures 1 and 2). These platforms are designed by Quanser (Mechatronics Control Kit Model M-1). They are composed of a 2 rigid-links, low-friction, and two joints. The parameters of the Pendubot system are: $a_1 = m_1 l_{c1}^2 + m_2 l_1^2 + I_1 = 0.0022$, $a_2 = m_2 l_{c2}^2 + I_2$=0.00101, $a_3 = m_2 l_1 l_{c2} = 0.0008$, $a_4 = m_1 l_{c1} + m_2 l_1 = 0.0182$, $a_5 = m_2 l_{c2} = 0.0065$, and the Rotatory pendulum parameters are: $b_1 = I_1 + m_2 l_1^2 = 0.0015$, $b_2 = m_2 l_2^2 = 0.0013$, $b_3 = m_2 l_1 l_2 = 0.0056$, $b_4 = I_2 + m_2 l_2^2 = 0.012$ and $b_5 = m_2 l_2 = 0.0055$. In both cases, m_i are the mass of ith link, l_i is the length of ith link, l_{ci} is the length to the center of the mass of the ith link, I_i is the inertia moment of ith link, $i = 1, 2$, $q_a \triangleq q_1$ and $q_u \triangleq q_2$, the

[¶]From Proposition 2.1, note that R is a diagonal matrix.

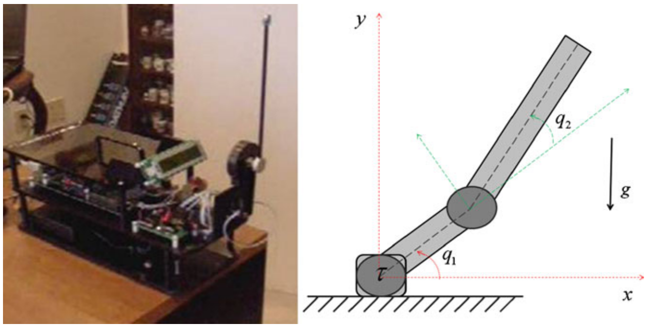

Figure 1. Pendubot.

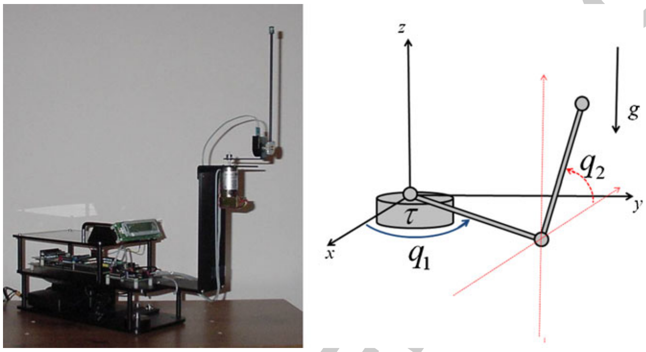

Figure 2. Rotatory pendulum.

Table I. Dynamics of the two underactuated robots.

Dynamic	Pendubot	Rotatory pendulum
d_{11}	$a_1+a_2+a_3\cos(x_2)$	$b_1+b_2\sin^2 x_2$
$d_{12}=d_{21}$	$a_2+a_3\cos(x_2)$	$b_3\cos x_2$
d_{22}	a_2	b_4
c_{11}	$-a_3\sin(x_2)x_3$	$\frac{1}{2}b_2\sin(2x_2)x_4$
c_{12}	$-a_3\sin(x_2)(x_3+x_4)$	$-b_3\sin x_2 x_4+\frac{1}{2}b_2\sin(2x_2)x_3$
c_{21}	$-a_3\sin(x_2)x_3$	$\frac{1}{2}b_2\sin(2x_2)x_3$
c_{22}	0	0
g_1	$a_4 g\cos(x_1)+a_5 g\cos(x_1+x_2)$	0
g_2	$a_5 g\cos(x_1+x_2)$	$-gb_5\sin x_2$

acceleration of gravity constant $g=9.81\,\mathrm{m/s^2}$, where subindexes 1 and 2 stand for the first and second link, respectively [10].

The system dynamics stated by (11) are given in Table I.

4.2. Firmware

A Digital Signal Processor C6713DSK board control system was integrated on a 16-bit expansion bus slot of a personal computer. The real-time toolbox compiler (MATLAB SIMULINK) provided the programming environment. The control input is transmitted to a 24Volt DC Motor with 1000 Cnt/Rev Optical Encoder from Pittman Inc., 24VDC at 2.1AMP power supply is employed from ELPAC Power Systems [10].

DOI: 10.1002/oca

Table II. Dynamics of $f(x)$ [6].

	Pendubot and rotatory pendulum
$f_1(x)$	x_3
$f_2(x)$	x_4
$f_3(x)$ $f_4(x)$	$D^{-1}(x_1)(-C(x)x_2 - G(x_1))$

Table III. Dynamics of $g(x)$ [6].

	Pendubot	Rotatory pendulum
$g_1(x)$	$\frac{a_2}{\det(D(x_1))}$	$\frac{b_1}{\det(D(x_1))}$
$g_2(x)$	$-\frac{a_2+a_3\cos x_2}{\det(D(x_1))}$	$\frac{-b_3\cos x_2}{\det(D(x_1))}$
$\det(D(x_1))$	$a_1a_2 + a_3^2\cos^2 x_2$	$b_4(b_1+b_2\sin^2 x_2) - b_3^2\cos^2 x_2$

Table IV. Parameters of A [6].

	Pendubot	Rotatory pendulum
e_{11}	$\frac{a_2a_4-a_3a_5}{a_1a_2-2a_3^2}g$	0
e_{12}	$\frac{-a_3a_5}{a_1a_2-2a_3^2}g$	$\frac{b_2}{b_1b_4-b_3^2}g$
e_{21}	$\frac{(a_1+a_3)a_5-(a_2+a_3)a_4}{a_1a_2-2a_3^2}g$	0
e_{22}	$\frac{(a_1+a_3)}{a_1a_2-2a_3^2}g$	$\frac{b_1+b_4}{b_1b_4-b_3^2}g$

4.3. Experimental conditions

The performance of the proposed controller in a physical experiment is shown against the implementation on a numerical simulation [9]. Experiments are carried out at high velocities to show the system controller performance at inertial dominated dynamics. In order to apply Proposition 2.1, let use take the linearized model $\dot{x} = Ax + Bu$, where B is obtained by Taylor series figured out on the desired upper unstable position.[‖]

From (11), the dynamics of $D(\cdot)$, $C(\cdot)$, and $G(\cdot)$ for the pendubot and rotatory pendulum systems correspond to Table I, and Equations (10) and (11). Or rewritten in a state space representation, functions $f(x)$ and $g(x)$ (as in (3)), have the dynamics given in Table II, III.

By taking the linearization of the former nonlinear system, at the top position (upper equilibrium point) of the corresponding system, the structure of the matrix A reads:

$$A = \begin{bmatrix} 0 & 0 & 1 & 0 \\ 0 & 0 & 0 & 1 \\ e_{11} & e_{12} & 0 & 0 \\ e_{21} & e_{22} & 0 & 0 \end{bmatrix},$$

where for each system, the matrix A is given in Table IV.

[‖]The pendubot top position is $(x_1, x_2, x_3, x_4) = (\pi/2, 0, 0, 0)$ and the Rotatory pendulum top position is $(x_1, x_2, x_3, x_4) = (0, 0, 0, 0)$.

DOI: 10.1002/oca

Table V. Parameters of B [6].

	Pendubot	Rotatory pendulum
$B_1(x)$	$\frac{a_2}{a_1 a_2 - 2a_3^2}$	$\frac{b_1}{b_1 b_4 - b_3^2}$
$B_2(x)$	$-\frac{a_2 + a_3 \cos x_2}{a_1 a_2 - 2a_3^2}$	$\frac{-b_3}{b_1 b_4 - b_3^2}$

Table VI. Numerical simulation.

Matrix	Pendubot	Rotatory pendulum
Q	diag$(8, 11.5, 5, 5)$	diag$(8, 11.5, 5, 5)$
R	2.5	2.5
k_E	49.8	10

Table VII. Experimental result.

Matrix	Pendubot	Rotatory pendulum
Q	diag$(6.87, 7.8, 4.5, 5.2)$	diag$(6.8, 8.5, 6.5, 6.55)$
R	2	2
k_E	12.5	8.6

And B follows:

$$B^{\mathrm{T}} = [0 \;\; 0 \;\; B_1 \;\; B_2].$$

For each system, B is given in Table V.

From (8), it follows:

$$-(k_{11}(\bar{x}) \;\; k_{12}(\bar{x}) \;\; k_{13}(\bar{x}) \;\; k_{14}(\bar{x}))\bar{x} \approx -\frac{1}{r_1} B^{\mathrm{T}} \bar{P} \bar{x}, \tag{15}$$

where $\bar{P} \in \mathbb{R}^{4\times 4}$, $\bar{P} = [\bar{P}_{11} \;\; \bar{P}_{12}; \bar{P}_{21} \;\; \bar{P}_{22}]$ and $\bar{P}_{11} \in \mathbb{R}^{2\times 2}$, $\bar{P}_{11} = [\bar{p}_{11} \;\; \bar{p}_{12}; \bar{p}_{21} \;\; \bar{p}_{22}]$, $\bar{P}_{12} = \bar{P}_{21}^{\mathrm{T}} = [\bar{p}_{13} \;\; \bar{p}_{14}; \bar{p}_{23} \;\; \bar{p}_{24}]$, $\bar{P}_{22} = [\bar{p}_{33} \;\; \bar{p}_{34}; \bar{p}_{43} \;\; \bar{p}_{44}]$, and $R \in \mathbb{R}^{1\times 1}$. Then,

$$-\frac{1}{r_1}[0 \;\; 0 \;\; B_1 \;\; B_2]\bar{P}\bar{x} = -(k_1 \;\; k_2 \;\; k_3 \;\; k_4)\bar{x} = -K\bar{x}, \tag{16}$$

and the two link underactuated system at the top position, with (14), can be approximated as:

$$(k_{11}(\bar{x}) \;\; k_{12}(\bar{x}) \;\; k_{13}(\bar{x}) \;\; k_{14}(\bar{x}))|_{f(\bar{x})\to f(0)} \approx (k_1 \;\; k_2 \;\; k_3 \;\; k_4), \tag{17}$$

where $\bar{x} = [\bar{x}_1, \bar{x}_2]^{\mathrm{T}} \in \mathbb{R}^{2n}$ (see Equation (4)), $(k_1, k_2, k_3, k_4) = K$ are obtained from the Riccati equation solution (for linear system, this is the LQR solution), and this solution gives the $\bar{p}_{13}$, $\bar{p}_{14}$, $\bar{p}_{23}$, $\bar{p}_{24}$, $\bar{p}_{33}$, $\bar{p}_{34}$, $\bar{p}_{43}$, and $\bar{p}_{44}$ values.

Since the solution of matrix $\bar{P}$ gives four equations and seven unknown parameters, let us fix up the following parameters, $\bar{p}_{13} = 5$, $\bar{p}_{24} = 2$ and $\bar{p}_{34} = 6$, and then, the parameters of matrix $\bar{P}$ are obtained as follows:

$$\bar{p}_{14} = \frac{(k_1 - \bar{p}_{13}B_1)}{B_2}, \quad \bar{p}_{33} = \frac{(k_3 - \bar{p}_{31}B_4)}{B_2}, \quad \bar{p}_{23} = \frac{(k_2 - \bar{p}_{24}B_4)}{B_3}, \quad \bar{p}_{44} = \frac{(k_4 - \bar{p}_{34}B_3)}{B_4}, \tag{18}$$

where

$$K = (k_1 \;\; k_2 \;\; k_3 \;\; k_4) = [0 \;\; 0 \;\; g_1(\bar{x}_1) \;\; g_2(\bar{x}_1)]\bar{P} \tag{19}$$

DOI: 10.1002/oca

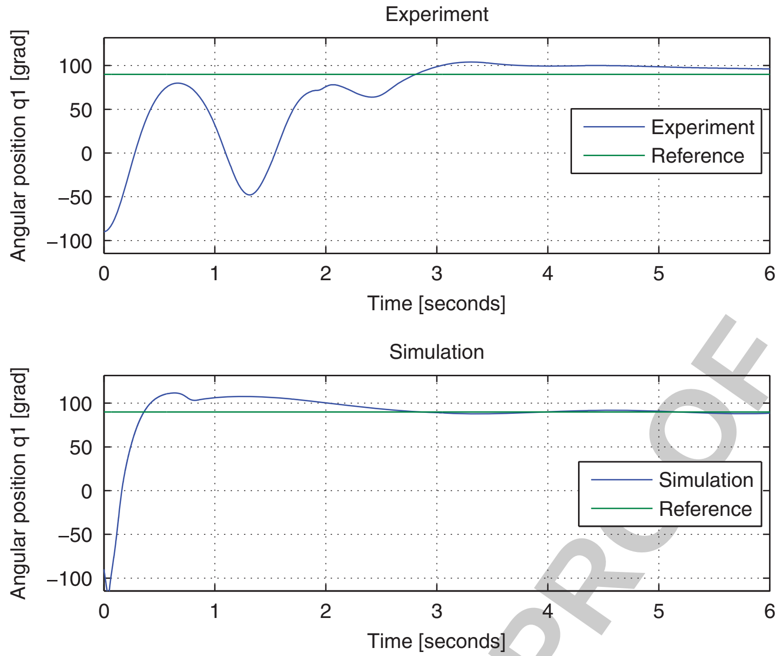

Figure 3. Pendubot: first link position.

Color Online, B&W in Print

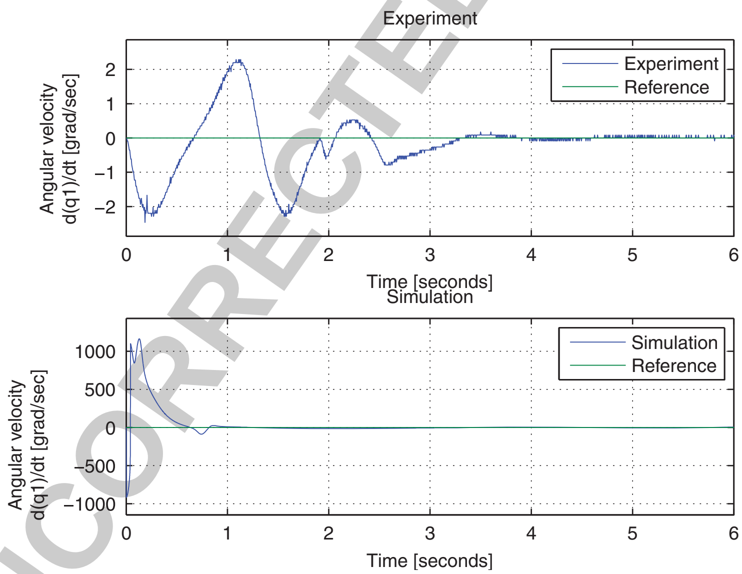

Figure 4. Pendubot: first link velocity.

Color Online, B&W in Print

and the parameters $\bar{p}_{11}=100$, $\bar{p}_{12}=0$, $\bar{p}_{21}=0$ and $\bar{p}_{22}=100$ are proposed such that the matrix $\bar{P}>0$.

The tuning of the gains is not easy and special attention must be paid to avoid misleading conclusions. Since a comparison between similar but structurally different dynamics are introduced, we assign the same value to the common gains. By taking the linearization of the system, linear gains for the LQR solution are obtained for the numerical simulation (Table VI) and for the experimental implementation (Table VII), and by trial error a feasible k_E gain is found. With these matrices given by Tables VI and VII, and the scalar gains there in, we finally show the

DOI: 10.1002/oca

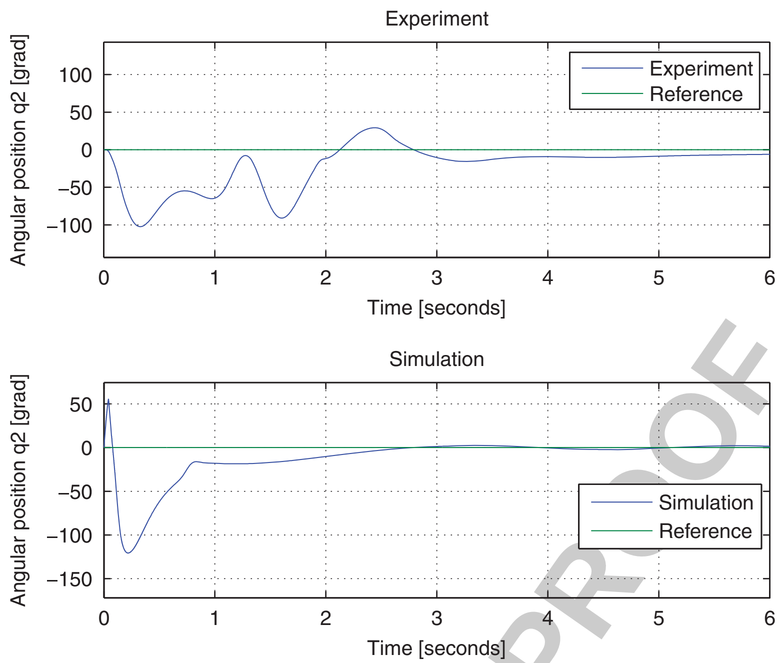

Figure 5. Pendubot: second link position.

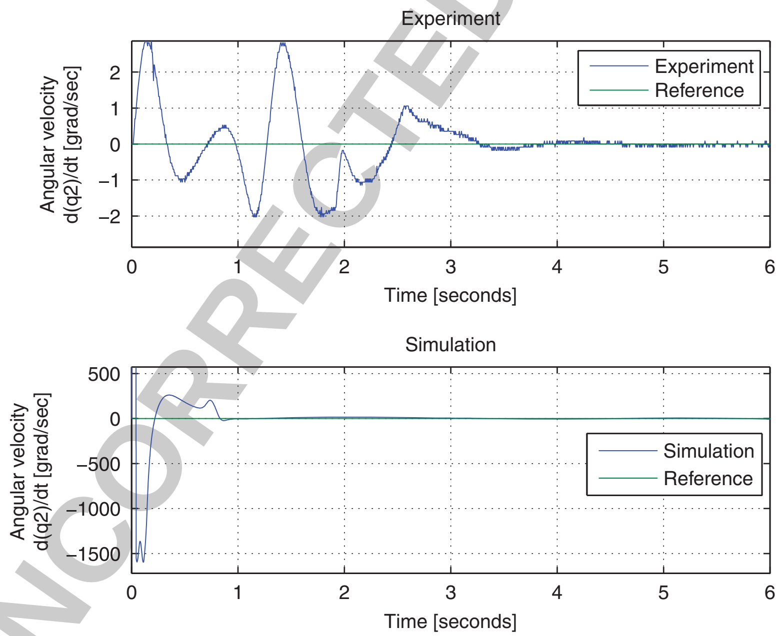

Figure 6. Pendubot: second link velocity.

numerical and the experimental results obtained by applying the control law (13). An analysis of the controlled system is shown in the following subsection.

4.4. Experiments

For a better visualization of the plots, some figures are shown in two subfigures. The initial conditions for both examples are given by the lower stable equilibrium point, i.e. the pendubot

DOI: 10.1002/oca

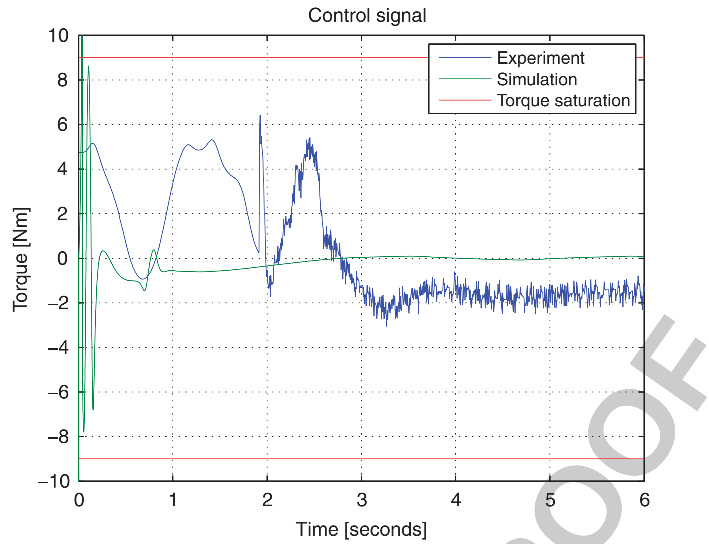

Figure 7. Pendubot: control signal.

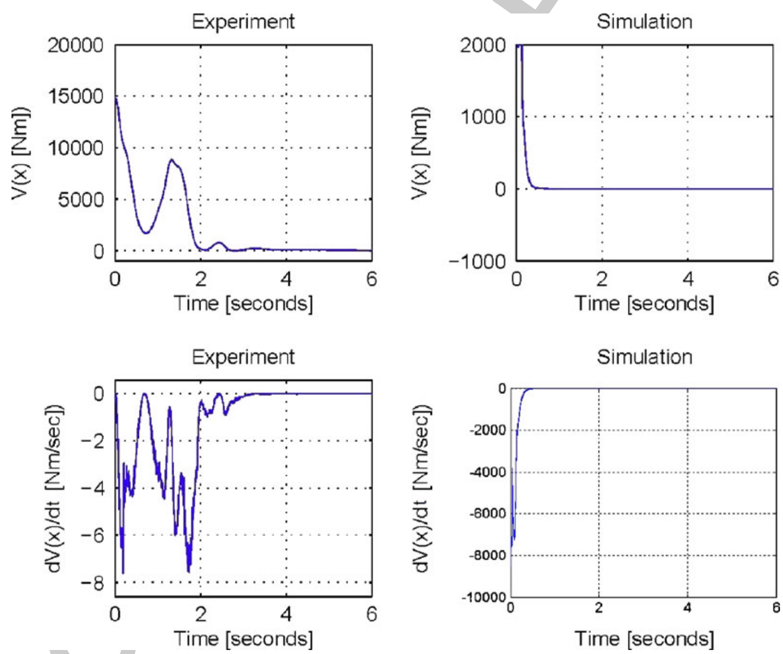

Figure 8. Pendubot: Lyapunov stability.

lower stable equilibrium point is $(x_1, x_2, x_3, x_4) = (-\pi/2, 0, 0, 0)$, the rotatory pendulum lower equilibrium point is $(x_1, x_2, x_3, x_4) = (\pi, 0, 0, 0)$, and the control objective is to follow the reference at the desired upper instable position, i.e. the pendubot top position is $(x_1, x_2, x_3, x_4) = (\pi/2, 0, 0, 0)$, the Rotatory pendulum top position is $(x_1, x_2, x_3, x_4) = (0, 0, 0, 0)$. For instance, in Figures 3, 5, 9, and 11, the subfigure 1 shows the experimental position in a time interval. Subfigure 2 shows the numerical simulation of position in some time interval. In Figures 4, 6, 10, and 12, the subfigure 1 shows the experimental velocity, whereas subfigure 2 shows the numerical simulation of velocity. The stability properties of numerical and experimental results are shown in Figures 8 and 14. The Figures 7 and 13 show the numerical and experimental control signal.

DOI: 10.1002/oca

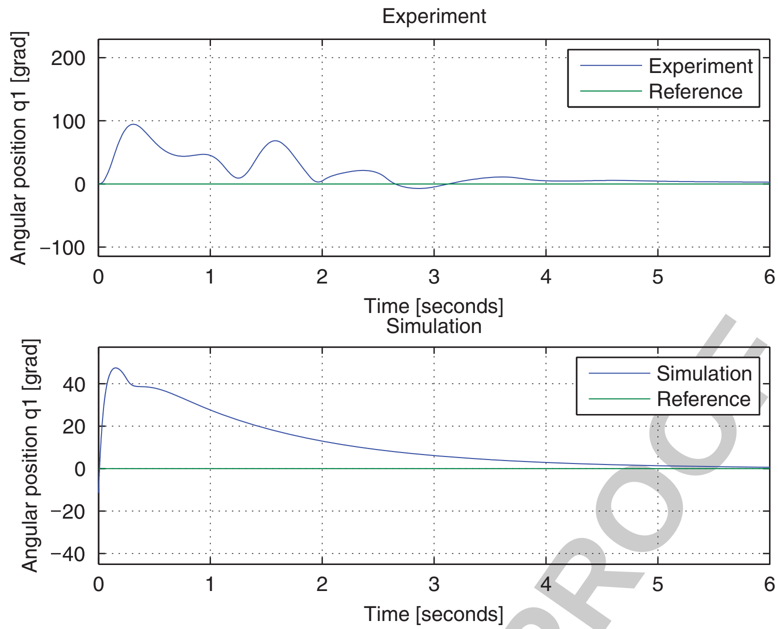

Figure 9. Rotatory pendulum: shoulder position.

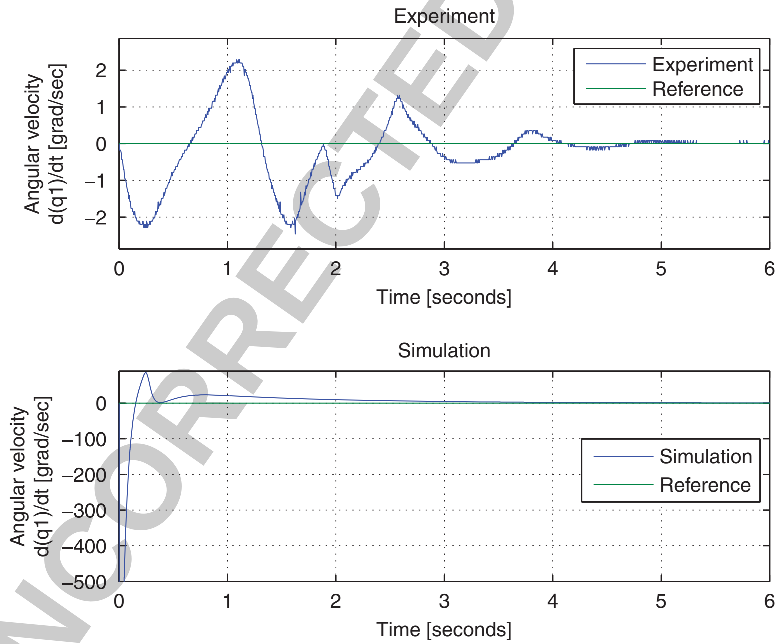

Figure 10. Rotatory pendulum: shoulder velocity.

Figures 3–6 shows how a dynamic displacement of the solution manifold converges to reference, i.e. the pendubot dynamics tends to upper unstable equilibrium position $x_1 \to \pi/2$, $x_2 \to 0$ $x_3 \to 0$, and $x_4 \to 0$. When a comparative plot of position errors is shown at high velocities of the numerical simulation and experiment, after a transient of 6 s, the numerical simulation yields an error whereas the experimental implementation reaches the reference about 3 s. However, a bigger joint velocity is displayed in the simulation, which implies more applied torque. Besides that, in the experimental implementation, a saturation threshold has been used (torque saturation is employed at ± 9.5 Nm,

DOI: 10.1002/oca

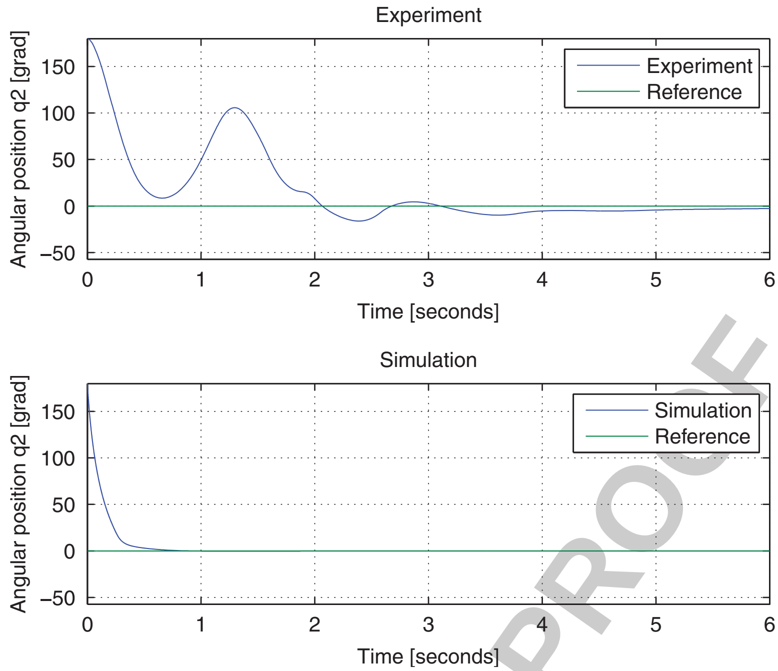

Figure 11. Rotatory pendulum: arm position.

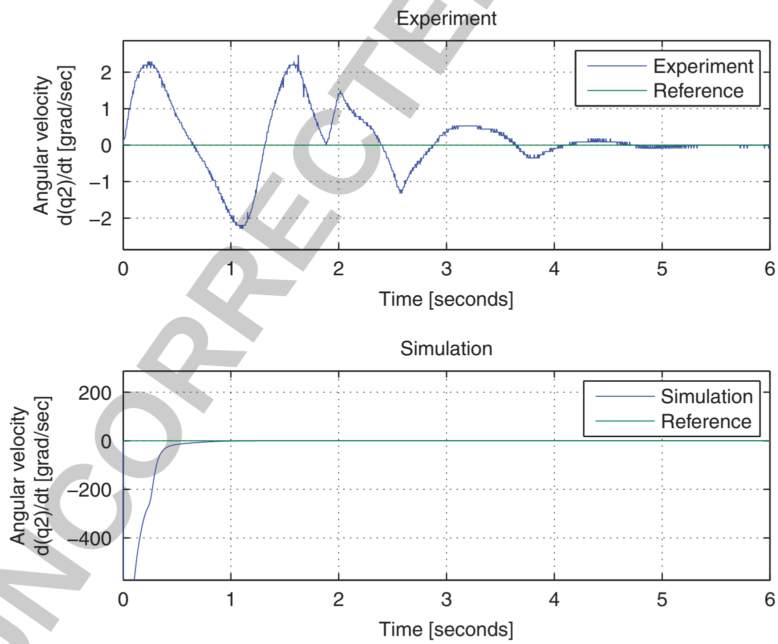

Figure 12. Rotatory pendulum: arm velocity.

see Figure 7). Figure 8 shows the controlled system asymptotic stability achieved via the Lyapunov function (4), the Lyapunov functions for each system are detailed in [9].

Main results of the rotatory pendulum system are presented in Figures 9–14. Figures 9 and 11 show the time evolution of articular position angles, which converge to top unstable configuration from initial conditions at 4 s. Figures 10 and 12 show how the articular velocities converge to

DOI: 10.1002/oca

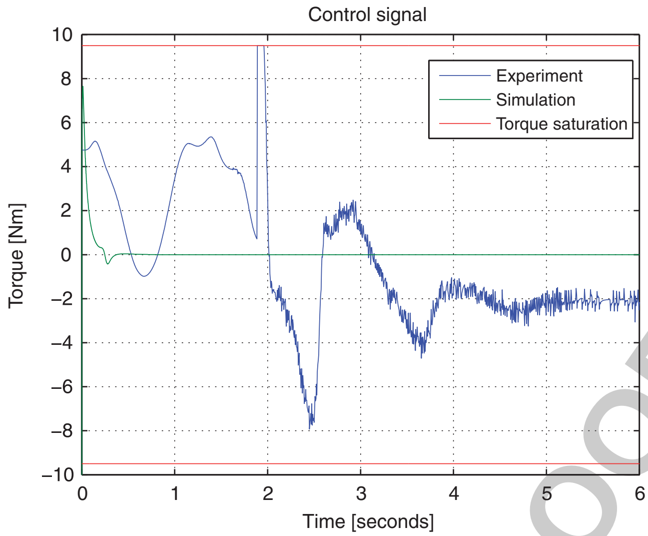

Figure 13. Rotatory pendulum: control signal.

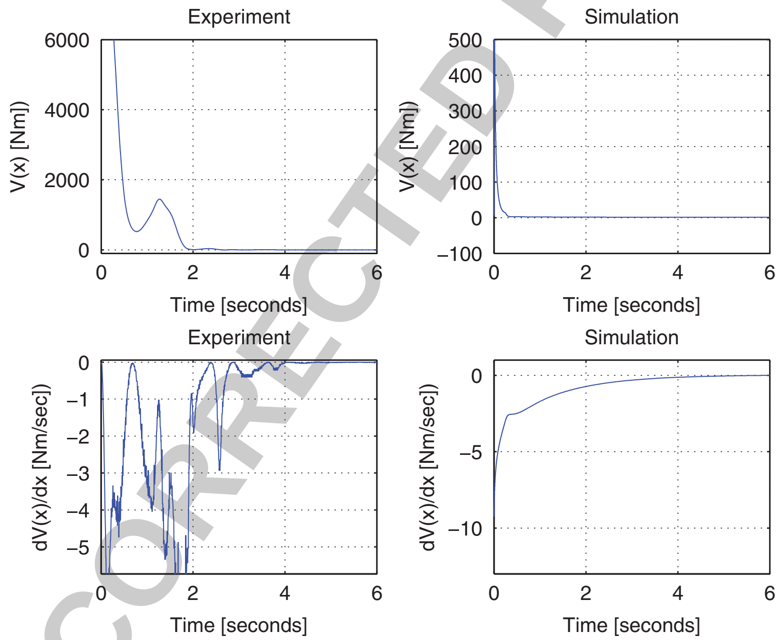

Figure 14. Rotatory pendulum: stability.

$(x_3 = 0,\ x_4 = 0)$. Applied torque is shown in Figure 13. Finally, Figure 14 shows the controlled system asymptotic stability achieved via the Lyapunov function (4).

Remark 4.1

The main reason why the experimental and simulation results do not present the same performance is because in the simulation we consider ideal conditions, i.e. we do not consider uncertain non-structured dynamics, such as tribology forces, disturbance, and others. Note that it is difficult to include these in the simulation, because they are uncertain. This problem can be seen in the tuning control gains as well, (Tables VI and VII).

DOI: 10.1002/oca

5. CONCLUSION

Experimental results of a class of underactuated robot control by using a sub-optimal controller are presented. Satisfactory results are obtained by applying the suboptimal nonlinear control law presented. By comparing it with some previous results, our proposal does not need to switch control laws when the system is near to the desired equilibrium point, and as the system approach to this equilibrium, the nonlinear control law becomes an LQR controller. By applying our generalized control law methodology, and by comparing a numerical simulation against a experimental implementation, control approach applied is illustrated.

ACKNOWLEDGEMENTS

The authors thank the anonymous reviewers for their valuable suggestions for improving this paper.

REFERENCES

1. Spong MW. Underactuated mechanical systems. In *Control Problems in Robotics and Automation*, Siciliano B, Valavanis KP (eds). Springer: London, U.K., 1997.
2. Fantoni I, Lozano R. *Non-linear Control for Underactuated Mechanical System*. Springer: Berlin, 2002.
3. Spong MW. The control of underactuated mechanical systems. *I Conferencia Internacional de Mecatrónica*, México D.F., Enero, 1994.
4. Park C, Scheeres DJ, Guibout V, Bloch A. Globally optimal feedback control law of the underactuatedheisenberg system by generating functions. *Proceedings of the 45th IEEE Conference on Decision and Control*. IEEE: San Diego, CA, U.S.A., 2006; 2687–2692.
5. Fantoni I, Lozano R, Spong MW. Energy based control of the Pendubot. *IEEE Transactions on Automatic Control* 2000; **45**(4):725–729.
6. Patricio Ordaz-Oliver J. Control basado en energía y estabilización para sistemas subactuados. *M.S. Thesis* (in Spanish), Pachuca, Hidalgo, 2007.
7. Rubi J, Rubio A, Avello A. Swing-up control problem for a self-erecting double inverted pendulum. *IEE Proceedings Control Theory and Applications* 2002; **149**(2):169–175.
8. Ma XQ, Shu C-Y. *Theory and Implementation of Fuzzy Control Scheme for Pendubot*. *Triennial World Congress*, Barcelona, Spain, 2002.
9. Patricio Ordaz-Oliver J, Santos-Sánchez OJ, López-Morales V. On the sub-optimal feedback control law synthesis of underactuated systems. *International Journal of Innovative Computing*, *Information and Control* 2009; **5**(9):2791–2808.
10. *Mechatronics Control Kit User's Manual*. Quanser, 2006.
11. Lewis FL. *Optimal Control*, School of Electrical Engineering, Georgia Institute of Technology, Atlanta Georgia, Wiley: New York. Q1
12. Kalman RE. When is a linear control system optimal? *Journal of Basic Engineering* 1964; **86**(1):51–60.
13. Bellman RE, Kalaba RE. *Dynamic Programming and Modern Control Theory*. Academic Press: New York, U.S.A., 1965. Q2

DOI: 10.1002/oca

Author Queries Form

John Wiley

JOURNAL TITLE: **OCA** **24/3/2011**

ARTICLE NO: 999

Queries and / or remarks

Query No.	Details required	Author's response
Q1	Please provide year for Ref. [11].	
Q2	Refs [11-13] are not cited in text. Please check.	